Published in final edited form as:
Cancer Discov. 2012 August ; 2(8): 722–735. doi:10.1158/2159-8290.CD-12-0014.

IDO is a nodal pathogenic driver of lung cancer and metastasis development

Courtney Smith[1,*], **Mee-Young Chang**[1,*], **Katherine Parker**[2], **Daniel Beury**[2], **James B. DuHadaway**[2], **Hollie E. Flick**[1,3], **Janette Boulden**[1], **Erika Sutanto-Ward**[1], **Alejandro Peralta Soler**[1,4], **Lisa D. Laury-Kleintop**[1], **Laura Mandik-Nayak**[1], **Richard Metz**[5], **Suzanne Ostrand-Rosenberg**[2], **George C. Prendergast**[1,6,7,†], and **Alexander J. Muller**[1,7,†]

[1]Lankenau Institute for Medical Research, Wynnewood PA USA

[2]Department of Biological Sciences, University of Maryland Baltimore County, Baltimore MD USA

[3]Department of Biochemistry, Drexel University College of Medicine, Philadelphia PA USA

[4]Richfield Laboratory of Dermatopathology, Cincinnati OH USA

[5]NewLink Genetics Corporation, Wynnewood PA USA

[6]Department of Pathology, Anatomy & Cell Biology, Thomas Jefferson University, Philadelphia PA USA

[7]Kimmel Cancer Center, Thomas Jefferson University, Philadelphia PA USA

Abstract

IDO (indoleamine 2,3-dioxygenase) enzyme inhibitors have entered clinical trials for cancer treatment based on preclinical studies indicating that they can defeat immune escape and broadly enhance other therapeutic modalities. However, clear genetic evidence of IDO's impact on tumorigenesis in physiologic models of primary or metastatic disease is lacking. Investigating the impact of *Ido1* gene disruption in mouse models of oncogenic KRAS-induced lung carcinoma and breast carcinoma-derived pulmonary metastasis, we have found that IDO-deficiency resulted in reduced lung tumor burden and improved survival in both models. Micro-CT imaging further revealed that the density of the underlying pulmonary blood vessels was significantly reduced in *Ido1*-nullizygous mice. During lung tumor and metastasis outgrowth, IL6 induction was greatly attenuated in conjunction with the loss of IDO. Biologically, this resulted in a consequential impairment of pro-tumorigenic MDSCs (myeloid-derived suppressor cells), as restoration of IL6 recovered both MDSC suppressor function and metastasis susceptibility in *Ido1*-nullizygous mice. Together, our findings define IDO as a prototypical integrative modifier that bridges inflammation, vascularization and immune escape to license primary and metastatic tumor outgrowth.

[†]Corresponding authors: Lankenau Institute for Medical Research, 100 Lancaster Avenue, Wynnewood PA 19096. Phone: 484.476.8034 or 8475. Fax: 484.476.8533. mullera@mlhs.org or prendergast@limr.org.
[*]These authors contributed equally to this study.

COMPETING FINANCIAL INTEREST

G.C.P., A.J.M. and J.B.D. declare a potential conflict of interest with regard to IDO due to intellectual property, financial interests, grant support, and consultancy roles with New Link Genetics Corporation, which is engaged in the clinical development of IDO inhibitors for the purpose of treating cancer and other diseases. R.M. is an employee of New Link Genetics Corporation and has financial and intellectual property interests in the company. The other authors have no competing financial interests to declare.

Keywords

Kras; lung cancer; breast cancer metastasis; mouse models; vascularization; immune escape; interleukin 6 (IL-6); myeloid-derived suppressor cells (MDSC)

INTRODUCTION

Inflammatory tissue microenvironments contribute strongly to tumor progression, but due to the complex multifactoral nature of inflammation there remains limited understanding of specific pathogenic components that might be targeted to effectively treat cancer (1). In this context, the tryptophan catabolizing enzyme IDO has emerged as an intriguing target implicated in tumoral immune escape (2, 3). IDO inhibitory compounds have entered clinical trials based on evidence of immune-based antitumor responses in a variety of preclinical models of cancer (4–10). Meanwhile, inadvertent IDO targeting may already be providing benefits to patients as illustrated by recent evidence that the clinically approved tyrosine kinase inhibitor imatinib dampens IDO induction as a key mechanism for achieving therapeutic efficacy in the treatment of gastrointestinal stromal tumors (11).

While results with IDO pathway inhibitors are provocative, the conclusions that can be drawn are inherently limited by drug specificity concerns, especially in the absence of independent genetic validation. Addressing this issue, our studies on the impact of *Ido1* gene deletion on DMBA/TPA-elicited skin papillomagenesis established that IDO has an integral tumor-promoting role in the context of phorbol ester-elicited inflammation (12, 13), but interpretation of these results is tempered by the possibility that the chemical exposures in this model may produce anomalies irrelevant to the majority of spontaneous tumors. The lungs present a particularly compelling physiological context in which to further investigate the role of IDO in tumorigenesis as IDO is known to be highly inducible in this tissue (14, 15) and there is an urgent unmet medical need for effective therapeutic options to treat primary lung tumors and metastases. In this report, we investigated the consequences of IDO loss through genetic ablation in the context of well-established, pulmonary models of oncogenic KRAS-induced adenocarcinoma and orthotopic breast carcinoma metastasis. Our findings reveal previously unappreciated roles for IDO in vascularization and in the production of the pro-inflammatory cytokine IL6 that in turn dictates the development of protumorigenic, myeloid-derived suppressor cells (MDSCs).

RESULTS

IDO-deficiency prolongs the survival of mice with sporadic *Kras*^{G12D}-driven lung carcinomas

LSL-Kras^{G12D} (*Lox-Stop-Lox Kras*^{G12D}) transgenic mice develop sporadic focal pulmonary adenocarcinomas following intranasal administration of *cre*-expressing adenovirus vector (Ad-*cre*) to activate the latent oncogenic *Kras*^{G12D} allele (16). These RAS-induced adenocarcinomas elicit a robust inflammatory response (17) wherein IDO may impart a pro-tumorigenic skew (2). To investigate this hypothesis in an autochthonous lung tumor setting we introduced *Ido1*$^{-/-}$ (homozygous *Ido1*-null) alleles (18) into the *LSL-Kras*^{G12D} mouse strain. *Ido1*$^{-/-}$ *Lox-Kras*^{G12D} mice displayed significantly increased survival relative to *Lox-Kras*^{G12D} mice at two different multiplicities of Ad-*cre* infection (Fig. 1A,B). Similar levels of *cre* were present in the lungs of both strains at 0, 1, 3 and 7 days post-infection (Fig. 1C). Unexpectedly, histopathological examination at 6 wk revealed that the frequency of early precancerous lesions was actually ~3-fold higher in the *Ido1*$^{-/-}$ *Lox-Kras*^{G12D} mice (Fig. 1D,E), substantiating that IDO-deficiency does not interfere at the stage of Ad-*cre*-mediated oncogenic RAS activation required to initiate these tumors (16) (Supplementary

Fig. S1A). While early tumorigenesis may be negatively impacted by IDO-mediated tryptophan catabolism, as previously proposed (19), this phenomena was transient with the differential no longer significant by 12 wks (Fig. 1E).

IDO-deficiency impairs tumor outgrowth and vascular development in the lung

To assess the impact of *Ido1*-loss on overt lung tumors, noninvasive micro-CT scans were performed on groups of *Lox-Kras*^{G12D} and *Ido1*$^{-/-}$ *Lox-Kras*^{G12D} mice at 18 and 24 wk following Ad-*cre* administration (Fig. 2A). Semi-automated quantitative image analysis (20) was performed on 3D reconstructions of the thoracic cavity excluding the heart to assess the combined tumor and vasculature volume within this space. While lung tumor burden did increase progressively in both cohorts, it was significantly reduced in the *Ido1*$^{-/-}$ *Lox-Kras*^{G12D} mice relative to the corresponding *Ido1*-competent *Lox-Kras*^{G12D} mice (Fig. 2B). Individual micro-CT scan images paired with 3D reconstructions of total chest space and functional lung volume visually highlight the difference in lung tumor burden between representative *Ido1*$^{-/-}$ *Lox-Kras*^{G12D} and *Kras*^{G12D} animals (Fig. 2A and Supplementary Videos). These results indicate that IDO-deficiency mitigates overt lung tumor outgrowth, consistent with the increased survival exhibited by these mice.

Micro-CT analysis additionally revealed that the density of normal vasculature in the lungs of uninfected animals was substantially diminished in the *Ido1*$^{-/-}$ animals (Fig. 2A,B). Intriguingly, the difference in vascular density between IDO-deficient and IDO-competent cohorts was proportionately comparable to the difference in overt lung tumor burden at the 18 and 24 wk time points (Supplementary Fig. S1B), suggesting an association between the extent of the underlying basal vasculature and the capacity of the lungs to support tumor formation. Immunofluorescent staining of blood vessels in the lungs confirmed the decrease in pulmonary vascular density in *Ido1*$^{-/-}$ animals (Fig. 2C). The area within the lungs occupied by vessels was reduced by about 1.6-fold in *Ido1*$^{-/-}$ animals (Fig. 2D), in line with the differential identified by micro-CT data analysis. Further analysis revealed that the reduction in vascular density occurred predominantly at the level of small to medium size vessels, which were nearly twice as abundant in the WT animals, while there was little difference in the number of large vessels (Fig. 2E and Supplementary Fig. S1C).

IDO promotes IL6 elevation during lung tumor formation

In the lungs, IDO is highly responsive to pathogen or cytokine exposure (14, 15). To determine whether lung tumorigenesis also stimulates IDO, we compared steady-state levels of the tryptophan catabolite kynurenine at various times after *Kras*^{G12D} activation. While baseline levels of kynurenine in the lungs of uninfected *Lox-Kras*^{G12D} mice were significantly higher than in their IDO-deficient counterparts (Fig. 3A), these levels remained constant during lung tumorigenesis (Fig. 3A). In contrast, a multiplexed analysis of inflammatory cytokines at 19 and 26 wks revealed IL6 to be elevated ~25- and 68-fold respectively in lungs from tumor-bearing *Lox-Kras*^{G12D} mice but only ~1- and 3-fold in *Ido1*$^{-/-}$ *Lox-Kras*^{G12D} mice (Fig. 3B). This finding was notable given the known tumor-promoting role of IL6 in this model (21). While not of the same magnitude, induction of CCL2/MCP1 (chemokine (C-C motif) ligand 2) was likewise attenuated in tumor-bearing *Lox-Kras*^{G12D} mice lacking *Ido1* (Fig. 3C). In contrast, *Ido1*-loss did not significantly affect the relative levels of IL10, IFNγ, TNFα or IL12p70 (data not shown).

IDO-deficiency impedes the development of pulmonary metastases

Given the evidence that *Ido1*$^{-/-}$ mice are resistant to the outgrowth of primary lung tumors, we asked whether *Ido1*$^{-/-}$ animals might exhibit reduced susceptibility to pulmonary metastasis development as well. This question was investigated by orthotopic engraftment of mice with highly malignant 4T1 breast carcinoma cells which metastasize efficiently to the

lungs. Survival was increased significantly in *Ido1*$^{-/-}$ hosts compared to WT hosts after challenge with either a 4T1-luciferase expressing subclone or with parental 4T1 cells despite an overall shift in the curves (Fig. 4A,B). No difference in primary tumor growth rate was observed (Supplementary Fig. S2A,B), but metastatic lung nodules at necropsy were unambiguously less pronounced in *Ido1*$^{-/-}$ mice (Fig. 4C). Non-invasive micro-CT imaging also confirmed a marked reduction in metastatic burden in *Ido1*$^{-/-}$ mice (Fig. 4C), which was quantified by an *ex vivo* colony forming assay (22) (Fig. 4D). The metastasis differential was not attributable to reduced intravasation because the same numbers of tumor cells were present in peripheral blood samples from both strains (Fig. 4D). In contrast to lung, no difference in metastatic burden was observed in liver, although the presence of 4T1 cells was also nearly too low to detect in this tissue (Supplementary Fig. S2C). Since excision of the primary tumor can alter immune-based effects on metastasis (23), we evaluated the metastasis burden in resected mice. *Ido1*$^{-/-}$ mice continued to exhibit significant resistance to metastasis development (Fig. 4E), indicating that IDO-mediated support of metastatic development in lung is not dependent on the presence of the primary tumor. We also examined pulmonary VEGF levels but found that these increased comparably in both WT and *Ido1*$^{-/-}$ lungs during metastasis development and were actually somewhat higher at baseline in the *Ido1*$^{-/-}$ lungs (Supplementary Fig. S2D).

IDO is activated during metastatic lung colonization and potentiates IL6 induction

In WT mice, IDO1 protein and kynurenine levels both increased in the lungs during 4T1 metastasis development, particularly at 5 and 6 wk post-engraftment (Fig. 5A,B). The principle source of IDO1 expression in this context appears to be the native stroma rather than the engrafted 4T1 tumor cells because no IDO1 protein was detectable in the lungs of *Ido1*$^{-/-}$ mice (Fig. 5A), even at 7 wk post-engraftment when the metastatic tumor burden was high. However, a weak but significant increase in kynurenine was observed in the lungs of *Ido1*$^{-/-}$ mice (Fig. 5B), suggesting that metastasis development may be associated with induction of an alternative mechanism of kynurenine production, such as IDO2 (24) or TDO2 (tryptophan 2,3-dioxygenase) (25), either in conjunction with or in the absence of IDO1.

As in the *Kras*-driven primary lung tumor model, *Ido1* competence in the pulmonary metastatic setting was linked to enhanced elevation of IL6, with levels increasing up to 15-fold over baseline in WT animals (Fig. 5C). On the other hand, the IL6 levels in *Ido*$^{-/-}$ lungs remained ~2 to 4-fold over baseline even when evaluated at an extended time point to account for the differential in tumor burden (Fig. 5C). Thus, like the autochthonous lung tumor studies, results from this lung metastasis model led us to infer a positive regulatory link between IDO and IL6 production. Direct interrogation of this hypothesis was carried out in a cell-based assay with known IDO inducers. LPS induced both IDO activity and IL6 production in monocytic U937 cells while IFNγ on its own elicited little response but greatly elevated the level of IDO activity in combination with LPS that was mirrored by a comparable enhancement of IL6 production (Fig. 6A). In both instances, inclusion of the competitive IDO inhibitory compound MTH-tryptophan (8) significantly suppressed the observed increases in IDO activity as well as IL6 production (Fig. 6A). MTH-tryptophan-mediated suppression of IL6 induction was confirmed in a second monocytic cell line HL-60 (Fig. 6B). Likewise, siRNA-mediated interference with *Ido1* gene expression also significantly suppressed IL6 induction (Fig. 6C). Taken together, these results are consistent with our *in vivo* findings suggesting that IDO activity can potentiate the elevated production of IL6.

IDO drives MDSC expansion and immunosuppressive function

Studies in *Il1r*$^{-/-}$ (IL1 receptor-nullizygous) mice have demonstrated a crucial role for IL6 in 4T1 pulmonary metastasis development (26). At the cellular level, IL1β enhances development of tumor-promoting MDSCs with IL6 serving as a critical downstream mediator of this process (26). Since *Ido1*-loss attenuated IL6 induction and metastatic colonization in the lung, we hypothesized that MDSCs may be compromised at some level in tumor-bearing *Ido1*$^{-/-}$ mice. MDSCs isolated from WT and *Ido1*$^{-/-}$ mice did not differ phenotypically (Fig. 7A and Supplementary Fig. S3A), however, an early delay in the expansion of $Gr1^+CD11b^+$ cells in *Ido1*$^{-/-}$ mice, similar to that observed in *Il1r*$^{-/-}$ animals (26), was noted (Fig. 7B). Moreover, circulating MDSCs isolated from *Ido1*$^{-/-}$ hosts were functionally impaired in their ability to suppress T cells (Fig. 7C). We did not detect IDO1 protein in $Gr1^+CD11b^+$ cells obtained from tumor-bearing WT hosts (Supplementary Fig. S3B) consistent with the hypothesis that the observed functional impairment of MDSCs is a non-cell autonomous effect of IDO-deficiency in which IL6 may act as a key intermediary.

IL6 is critical to IDO-driven MDSC activity and pulmonary metastasis

To directly test the ability of IL6 to functionally restore MDSC suppressive activity in *Ido1*$^{-/-}$ mice, orthotopic tumors were established using 4T1-IL6 cells (26), a 4T1 cell population engineered to constitutively express IL6. MDSCs isolated from *Ido1*$^{-/-}$ mice engrafted with 4T1-IL6 cells exhibited an elevated T cell suppressive activity similar to that of MDSCs isolated from WT hosts engrafted with parental 4T1 cells (Fig. 7D). Further enhancement of MDSC-suppressive activity could be achieved by engrafting 4T1-IL6 cells into WT mice (Fig. 7D), indicating that the endogenous IL6 levels stimulated by parental 4T1 tumor cells in WT animals were not fully saturating with regard to promoting MDSC suppressor function.

We next asked whether restoring IL6 levels could also reverse the metastatic resistance exhibited by *Ido1*$^{-/-}$ mice. In the orthotopic setting, high levels of IL6 produced in primary tumors formed by 4T1-IL6 cells complicated the analysis by impairing the efficiency of pulmonary metastasis (possibly reflecting the recruitment of metastatic cancer cells back to IL6-expressing primary tumors as documented previously (27)). However, since our results in orthotopically engrafted mice had indicated that the *Ido1* allelic status does not affect 4T1 intravasation, we reasoned that a valid assessment of the impact of IDO deficiency on pulmonary metastasis could be made by introducing the metastatic tumor cells directly into the circulation. Accordingly, we confirmed that intravenously engrafted *Ido1*$^{-/-}$ mice maintained their resistance to pulmonary metastasis formation, with the apparent mean metastatic tumor burden being 30.4-fold and 31.6-fold lower in *Ido1*$^{-/-}$ versus WT mice challenged with 4T1 and 4T1-IL6 cells respectively (Fig. 7E). The proportional increase in metastatic burden observed in the 4T1-IL6 challenged cohorts is also in line with the proposed interpretation of the MDSC functional data that IL6 is not being produced at saturating levels in the 4T1-challenged WT animals. Due to the significantly higher metastasis burden produced by 4T1-IL6 tumors in *Ido1*$^{-/-}$ mice, comparison to WT mice challenged with 4T1 tumors yielded a differential in mean metastatic tumor burden of only 4.8-fold (Fig. 7E). Thus, IL6 supplementation not only rescued WT levels of MDSC suppressor function in 4T1 tumor-challenged *Ido1*$^{-/-}$ mice, but also markedly restored their susceptibility to pulmonary metastasis development.

DISCUSSION

The idea of immune escape as a ‘hallmark of cancer’ (28, 29) represents a groundbreaking though still largely untested paradigm within the field of cancer biology. The presumption that tumors exploit IDO activity as a mechanism of immune escape, initially inferred from

the pioneering studies on maternal immune tolerance of Munn et al. (30), has become increasingly accepted despite a fundamental deficit in genetic support for IDO's role in tumor development. The current study addresses this gap with direct genetic validation of IDO's importance in well established models of lung cancer and metastasis that offers novel insights into IDO's impact on tumor pathogenesis. Moreover, these findings strongly encourage the prioritization of clinical investigations into the use of IDO pathway inhibitors for treating lung adenocarcinomas and pulmonary metastases where more effective modalities are urgently needed.

While IDO activity was not elevated in lung tissue beyond baseline levels during KRAS-driven lung tumor development, the observed reduction in pulmonary vascularization in *Ido1*$^{-/-}$ animals even prior to initiation of tumorigenesis implied that the loss of steady state IDO in this context was sufficiently consequential to impact physiological processes important to tumor outgrowth. Enhanced tumor vascularization has been reported in tumor xenograft models involving exogenous IDO overexpression (31, 32), but our study is the first to identify a role for IDO in supporting vascular development under native physiological conditions. Our findings likewise genetically establish the importance of IDO activity in non-tumor cells for supporting pulmonary metastasis. In this manner, IDO activity may influence metastatic dissemination to tissues like the lung where its expression is particularly robust. This may, however, be less relevant when IDO (or tryptophan 2,3-dioxygenase (25)) activity is substantially elevated within the tumor cells themselves (8, 33), enabling the malignancy to preemptively shape its surroundings through intrinsic tryptophan catabolism. As such, IDO activity that originates from stromal cells of the tumor microenvironment or from the tumor cells themselves may contribute to directing tumor outgrowth.

The positive association between IDO and IL6 in lung tumorigenesis and metastasis was not necessarily anticipated given that it runs counter to expectations based on IDO-mediated induction of LIP, a negative regulatory isoform of the *Il6* gene expression promoting transcription factor C/EBPβ (24, 34). The precise regulatory impact of LIP on *Il6* expression is not clear cut, however, insofar as other findings have indicated that LIP can interact with NFκB to induce rather than limit *Il6* transcription (35). Our findings are also consistent with evidence that a downstream product of IDO-mediated catabolism, kynurenic acid, can potentiate IL6 production in the context of inflammation by signaling through the aryl hydrocarbon receptor (36). IL6 is a pleiotropic cytokine that is widely implicated in supporting neoplastic outgrowth in the context of chronic inflammation (37). Clinically, IL6 has been established as a marker of early relapse of resected lung tumors (38). Analyses of DNA polymorphisms in the IL6 promoter region have identified positive correlations between IL6-inducibility and lung cancer susceptibility in the context of concurrent inflammatory disease (39) as well as micrometastatic disease in high-risk breast cancer patients (40). Functionally, IL6 induction has been identified as an essential downstream component of RAS-induced tumorigenesis (41) that is directly linked to lung tumor development in the *Lox-Kras*^{G12D} transgenic mouse model (21). Numerous other studies indicate that IL6 can also contribute to tumor promotion by supporting angiogenesis and neovascularization of tumors (42, 43). Thus biologically, the epidemiological and functional data for IL6 are consistent with the tumor-promoting activity that we have ascribed to IDO through mouse genetics.

Tumor responses to IDO inhibitory compounds require functional host immunity (5, 6, 8, 9), but the mechanisms through which IDO promotes immune escape have yet to be fully delineated. Connecting IL6 to IDO provides valuable insight in this regard. IL6 has previously been identified in the 4T1 metastasis model as critical to the induction of MDSCs, which act as potent inhibitors of antitumor immunity (44). MDSC accumulation is

known to be driven by several factors that are produced by tumor cells and the tumor stroma, including the potent inflammatory mediators prostaglandin E2 and IL1β (interleukin-1β) (45–47). Genetic ablation of IL1β signaling can affect both the early accumulation of MDSCs as well as their immune suppressive capability (26), and IL6 has been determined to be a downstream mediator for the effects of IL1β on MDSC populations in tumor-bearing animals (26). In this context, our findings identify IDO as a key determinant of IL6-elicited MDSC accumulation and suppressor activity. Interestingly, IL1β may dynamically potentiate IDO's contribution to IL6 induction given that IL1β can promote the upregulation of IFNGR1 (interferon-γ receptor 1) (48) which enhances *Ido1* inducibility in response to IFNγ. In contrast, IL6 may exert a counterregulatory feedback effect by inducing SOCS3 (suppressor of cytokine signaling 3), which not only attenuates IL6 signaling (49) but also limits IDO transcription and IDO enzyme stability (50, 51). Thus, IDO is well situated to act as a dynamic modifier of inflammatory states in the microenvironment of primary tumors or budding metastases.

Our results deepen the concept that IDO activity profoundly influences the pathogenic character of the tumor microenvironment by identifying the cytokine IL6 as a crucial IDO effector for establishing 'cancer-associated' inflammation. IL6 is a far-reaching, pleiotropic signaling molecule that can elicit both intrinsic and extrinsic effects on tumor development (i.e. increased malignancy and survival as well as increased angiogenesis and immune escape). The ramifications of our results thus extend beyond the constrained effects that local IDO-mediated tryptophan catabolism might exert on the proximal microenvironment, and one would expect the potentiation of IL6 expression by IDO to affect diverse aspects of tumor development with the relative weighting of each aspect being an important focus of future study. Indeed, further investigations of IDO as a nexus for control of tumorigenic inflammation, vascularization and immune escape will be invaluable in formulating rational strategies to guide the best application of IDO inhibitors that have entered clinical development.

MATERIALS AND METHODS

Transgenic mouse strains

Congenic *Ido1*$^{-/-}$ mice on C57BL/6 and BALB/c strain backgrounds were provided by A. Mellor (GHSU) and corresponding control strains purchased from Jackson Laboratory. *LSL-Kras*^{G12D} Cre-inducible transgenic mice on a mixed 129SvJ-C57BL/6 strain background (16) were obtained through the Mouse Models of Human Cancer Consortium (NCI-Frederick). Administration of Ad-*cre* virus to activate the latent *Kras*^{G12D} allele in lungs of *LSL-Kras*^{G12D} transgenic mice (referred to as *Lox-Kras*^{G12D} mice (16)) was carried out as described (52). Doubly mutant *Ido1*$^{-/-}$ *LSL-Kras*^{G12D} mice were generated through breeding of the two transgenic strains. Mating pairs of BALB/c and T cell receptor (TcR) transgenic DO11.10 BALB/c mice (I-A^{d}-restricted, specific for chicken ovalbumin$_{323–339}$) were obtained from The Jackson Laboratory. Mating pairs of T cell receptor (TcR) transgenic Clone 4 BALB/c mice (H-2K^{d}-restricted, specific to influenza hemagglutinin (HA) peptide$_{518–526}$) and TcR transgenic TS1 BALB/c mice (I-E^{d}-restricted, specific to HA peptide$_{110–119}$) were provided by E. Fuchs (Johns Hopkins). All procedures involving mice were approved by either the LIMR or UMBC IACUC.

Micro-CT scanning

Three-dimensional micro-CT (computed tomography) images were acquired from anesthetized mice using an Impek Micro-CT scanner operated at 40kVp, 500-μA, 250-millisecond per frame, 5 frames per view, 360 views, and 1° increments per view. Contiguous axial DICOM-formatted images through each mouse thorax, with voxels of

dimensions 91μm×91μm×91μm were compiled into 3D format using Amira v5.1 software and normalized to Hounsfield units. Using the segmentation editor, manual selections of the chest cavity minus the heart were performed on every other slice followed by interpolation of these selections. Magic wand tool selection was performed at the threshold range defining air (determined to be between −750 and −350) to define the functional lung volume which was automatically subtracted from the total chest space to identify the volume representing vasculature and tumors (20).

4T1 tumor cell metastasis

Parental 4T1 mouse mammary carcinoma cells and 4T1-derived cell lines expressing luciferase (4T1-luc) or mouse *Il6* (4T1-IL6) were maintained as described (5, 22, 26). Primary tumor growth was monitored by caliper measurements of orthogonal diameters. Tumor volume was calculated using the formula for determining a prolapsed elliptoid ($[d^2 \times l] / 0.52$), where d is the shorter of the two orthogonal measurements. To enhance visualization of metastatic nodules, lungs were insuflated with India Ink dye, washed, and bleached in Fekete's solution. The clonogenic assay to assess metastatic burden was performed as described (22).

Real-time PCR

Lung DNA was analyzed by Real Time-PCR containing SYBR green PCR master mix (Applied Biosystems) and primers to amplify *cre* (5'-GGAGCCGCGCGAGATA-3' and 5'-GCCACCAGCTTGCATGATC-3') and endogenous mouse *Cd81* (5'-TCGCCAAGGATGTGAAGCA-3' and 5'-CATTGTTGGCATCATCATCCA-3'). Assays were performed in quadruplicate and relative quantitation of the viral *cre* gene present in lung tissue was calculated using the comparative threshold cycle (C_T) method (User Bulletin 2, Applied Biosystems) normalizing the target CT values to the internal housekeeping gene (*Cd81*).

Histology

Tissues were isolated and fixed in 10% neutral buffered formalin or 4% paraformaldehyde, sectioned, and stained for histopathological analysis with hemotoxylin and eosin using standard methods. For immunofluorescent staining, 4-μm paraffin sections were deparaffinized in xylene and rehydrated with a graded alcohol series. Following antigen retrieval (Vector), sections were washed and placed in 0.1% Triton for 10 minutes. Tissue was blocked in 40 μg/ml goat anti-mouse IgG-Fab (H+L) (Jackson ImmunoResearch) followed by 10% normal goat serum (Jackson Immunoresearch). Rabbit anti-mouse caveolin-1 (1:200) (Cell Signaling) was incubated overnight at 4°C. Sections were washed and incubated with goat anti-rabbit Cy3 (1:200) (Jackson ImmunoResearch). Tissues were mounted using Prolong Gold with DAPI (Invitrogen). To quantitate the blood vessel areas present within defined fields of caveolin-1 stained lung samples, four images were acquired per mouse from 5 WT and 5 $Ido1^{-/-}$ mice. Vessel boundaries were identified by caveolin-1 staining and the area of every vessel within each field was determined using AxioVision Release 4.6 software.

IP-Western blot analysis

Immunoprecipitation of IDO1 protein from mouse lung tissue with purified rabbit polyclonal antibody (7) followed by Western blot-based detection with rat monoclonal antibody (clone mIDO-48; Biolegend) was performed as described (9).

Flow cytometry for cytokine and cell analysis

Flow cytometry data were acquired on a FACSCanto II or Cyan ADP flow cytometer and analyzed using FACSDIVA (BD Biosciences) or Summit v4.3.02 (Beckman/Coulter) software. Multiplexed cytokine analysis was performed using the Inflammation Bead Array (BD Biosciences). Lung homogenates were centrifuged and supernatant added to beads in the array according to the manufacturer's instructions. Flow cytometry analysis of MDSCs harvested from digested lung samples or from blood was performed with the following antibodies as indicated: Gr1-FITC, Ly6G-PE, Ly6C-FITC, CD124 (IL-4Rα)-PE (BD Biosciences), CD11b-PacB, CD115-PE, F4/80-PE (BioLegend), Ly6C-PerCP (eBioscience), arginase, iNOS (BD Transduction Labs). Second step goat-anti-mouse IgG-Alexa 647 for arginase and iNOS was from Invitrogen. Isotype control antibodies were from BD Biosciences.

Kynurenine assay

Lungs were homogenized in PBS containing DTT and protease and phosphatase inhibitors (1:3 wt/vol). Deproteinated lysates were analyzed by HPLC coupled to electrospray ionization tandem mass spectroscopy (LC/MS/MS) analysis as described (9).

Cell culture

U937 and HL-60 monocytic cell lines (ATCC) were expanded for frozen storage after receipt and freshly thawed cells cultured in DMEM + 10% fetal bovine serum were used at early passage for experiments. No additional authentication was performed by the authors. 24 hour treatment of cells with LPS (100 ng/ml; Sigma) and/or IFNγ (100 ng/ml; R&D Systems) was carried out in triplicate on 1×10^4 cells per well in a 96-well dish. MTH-Trp (methylthiohydantoin-DL-tryptophan; 100 μmol/l; Sigma) was also included at the time of induction as indicated. Kynurenine and IL6 levels in the supernatant were analyzed as described above. *Ido1* gene 'knockdown' studies were performed with siRNAs (Dharmacon) targeting *Ido1* (Cat.# E-010337-00) or *Gapdh* (Cat.# D-001930-01) using the Accell siRNA Delivery System (Dharmacon) as described by manufacture. HL-60 cells were plated at 1×10^4 per well in a 96-well dish and cultured with 1% FBS in the Accell growth media. 24 hour treatment of cells with LPS and IFNγ was initiated at 48 hours following incubation with siRNA. Western blotting to detect IDO1 protein in cell lysates was performed following standard procedures using rabbit polyclonal anti-IDO1 (7) and rabbit monoclonal anti-β-actin (13E5; Cell Signaling) as a loading control. Detection was carried out with goat anti-rabbit IgG, HRP-linked secondary antibody (Cat.# 7074; Cell Signaling) using the SuperSignal West Femto Chemiluminescent substrate (Thermo Scientific).

T cell suppression assay

MDSC suppressive activity was measured as previously described (53) using transgenic splenocytes and their cognate peptides in the presence of 25-Gy irradiated, blood-derived MDSCs from 4T1 tumor-bearing mice. $HA_{518–526}$ $HA_{110–119}$ and $Ova_{323–339}$ peptides were synthesized in the Biopolymer Core Facility at the University of Maryland, Baltimore. ELISA duo set mAbs for mIL6 were from R&D Systems. Monoclonal antibody Vβ8.1,8.2-PE was from BD PharMingen.

Supplementary Material

Refer to Web version on PubMed Central for supplementary material.

Acknowledgments

We thank Gwen Guillard for tissue sectioning and histology and Lingling Yang for preliminary studies on MDSCs in IDO-deficient mice.

GRANT SUPPORT

A.J.M. is the recipient of grants from Susan G. Komen for the Cure and the W. W. Smith Foundation. G.C.P. is the recipient of NIH grants CA109542, CA159337 and CA159315 with additional support from NewLink Genetics Corporation, the Sharpe-Strumia Foundation, the Lankenau Medical Center Foundation and the Main Line Health System. S.O.R. is the recipient of NIH grants RO1CA115880, RO1CA84232, and RO1GM021248. C.S. is the recipient of a Postdoctoral Fellowship through the Department of Defense Breast Cancer Research Program. D.B. is the recipient of a Predoctoral Fellowship through the Department of Defense Breast Cancer Research Program.

REFERENCES

1. Peek RM Jr, Mohla S, DuBois RN. Inflammation in the genesis and perpetuation of cancer: summary and recommendations from a national cancer institute-sponsored meeting. Cancer Res. 2005; 65:8583–8586. [PubMed: 16204020]
2. Muller AJ, Mandik-Nayak L, Prendergast GC. Beyond immunosuppression: reconsidering indoleamine 2,3-dioxygenase as a pathogenic element of chronic inflammation. Immunotherapy. 2010; 2:293–297. [PubMed: 20635895]
3. Muller AJ, Scherle PA. Targeting the mechanisms of tumoral immune tolerance with small-molecule inhibitors. Nat Rev Cancer. 2006; 6:613–625. [PubMed: 16862192]
4. Banerjee T, DuHadaway JB, Gaspari P, Sutanto-Ward E, Munn DH, Mellor AL, et al. A key in vivo antitumor mechanism of action of natural product-based brassinins is inhibition of indoleamine 2,3-dioxygenase. Oncogene. 2008; 27:2851–2857. [PubMed: 18026137]
5. Hou DY, Muller AJ, Sharma MD, DuHadaway J, Banerjee T, Johnson M, et al. Inhibition of indoleamine 2,3-dioxygenase in dendritic cells by stereoisomers of 1-methyl-tryptophan correlates with antitumor responses. Cancer Res. 2007; 67:792–801. [PubMed: 17234791]
6. Kumar S, Malachowski WP, Duhadaway JB, Lalonde JM, Carroll PJ, Jaller D, et al. Indoleamine 2,3-Dioxygenase Is the Anticancer Target for a Novel Series of Potent Naphthoquinone-Based Inhibitors. J Med Chem. 2008; 51:1706–1718. [PubMed: 18318466]
7. Metz R, Duhadaway JB, Rust S, Munn DH, Muller AJ, Mautino M, et al. Zinc protoporphyrin IX stimulates tumor immunity by disrupting the immunosuppressive enzyme indoleamine 2,3-dioxygenase. Mol Cancer Ther. 2010; 9:1864–1871. [PubMed: 20530717]
8. Muller AJ, Duhadaway JB, Donover PS, Sutanto-Ward E, Prendergast GC. Inhibition of indoleamine 2,3-dioxygenase, an immunoregulatory target of the cancer suppression gene Bin1, potentiates cancer chemotherapy. Nat Med. 2005; 11:312–319. [PubMed: 15711557]
9. Muller AJ, DuHadaway JB, Jaller D, Curtis P, Metz R, Prendergast GC. Immunotherapeutic suppression of indoleamine 2,3-dioxygenase and tumor growth with ethyl pyruvate. Cancer Res. 2010; 70:1845–1853. [PubMed: 20160032]
10. Koblish HK, Hansbury MJ, Bowman KJ, Yang G, Neilan CL, Haley PJ, et al. Hydroxyamidine inhibitors of indoleamine-2,3-dioxygenase potently suppress systemic tryptophan catabolism and the growth of IDO-expressing tumors. Mol Cancer Ther. 2010; 9:489–498. [PubMed: 20124451]
11. Balachandran VP, Cavnar MJ, Zeng S, Bamboat ZM, Ocuin LM, Obaid H, et al. Imatinib potentiates antitumor T cell responses in gastrointestinal stromal tumor through the inhibition of Ido. Nat Med. 2011; 17:1094–1100. [PubMed: 21873989]
12. Muller AJ, Duhadaway JB, Chang MY, Ramalingam A, Sutanto-Ward E, Boulden J, et al. Non-hematopoietic expression of IDO is integrally required for inflammatory tumor promotion. Cancer Immunol Immunother. 2010; 59:1655–1663. [PubMed: 20640572]
13. Muller AJ, Sharma MD, Chandler PR, Duhadaway JB, Everhart ME, Johnson BA 3rd, et al. Chronic inflammation that facilitates tumor progression creates local immune suppression by inducing indoleamine 2,3 dioxygenase. Proc Natl Acad Sci USA. 2008; 105:17073–17078. [PubMed: 18952840]

14. Yoshida R, Imanishi J, Oku T, Kishida T, Hayaishi O. Induction of pulmonary indoleamine 2,3-dioxygenase by interferon. Proc Natl Acad Sci USA. 1981; 78:129–132. [PubMed: 6165986]
15. Yoshida R, Urade Y, Tokuda M, Hayaishi O. Induction of indoleamine 2,3-dioxygenase in mouse lung during virus infection. Proc Natl Acad Sci USA. 1979; 76:4084–4086. [PubMed: 291064]
16. Jackson EL, Willis N, Mercer K, Bronson RT, Crowley D, Montoya R, et al. Analysis of lung tumor initiation and progression using conditional expression of oncogenic K-ras. Genes and Development. 2001; 15:3243–3248. [PubMed: 11751630]
17. Ji H, Houghton AM, Mariani TJ, Perera S, Kim CB, Padera R, et al. K-ras activation generates an inflammatory response in lung tumors. Oncogene. 2006; 25:2105–2112. [PubMed: 16288213]
18. Baban B, Chandler P, McCool D, Marshall B, Munn DH, Mellor AL. Indoleamine 2,3-dioxygenase expression is restricted to fetal trophoblast giant cells during murine gestation and is maternal genome specific. J Reprod Immunol. 2004; 61:67–77. [PubMed: 15063630]
19. Ozaki Y, Edelstein MP, Duch DS. Induction of indoleamine 2,3-dioxygenase: a mechanism of the antitumor activity of interferon gamma. Proc Natl Acad Sci USA. 1988; 85:1242–1246. [PubMed: 3124115]
20. Haines BB, Bettano KA, Chenard M, Sevilla RS, Ware C, Angagaw MH, et al. A quantitative volumetric micro-computed tomography method to analyze lung tumors in genetically engineered mouse models. Neoplasia. 2009; 11:39–47. [PubMed: 19107230]
21. Ochoa CE, Mirabolfathinejad SG, Ruiz VA, Evans SE, Gagea M, Evans CM, et al. Interleukin 6, but not T helper 2 cytokines, promotes lung carcinogenesis. Cancer Prev Res (Phila). 2011; 4:51–64. [PubMed: 21098042]
22. Pulaski, BA.; Ostrand-Rosenberg, S. Mouse 4T1 breast tumor model. In: Coligan, JE.; Kruisbeek, AM.; Margulies, DH.; Shevach, EM.; Strober, W., editors. Current Protocols in Immunology. New York: John Wiley & Sons, Inc; 2000. p. 20.2.1-20.2.16.
23. Ostrand-Rosenberg S, Clements VK, Terabe M, Park JM, Berzofsky JA, Dissanayake SK. Resistance to metastatic disease in STAT6-deficient mice requires hemopoietic and nonhemopoietic cells and is IFN-gamma dependent. J Immunol. 2002; 169:5796–5804. [PubMed: 12421960]
24. Metz R, Duhadaway JB, Kamasani U, Laury-Kleintop L, Muller AJ, Prendergast GC. Novel tryptophan catabolic enzyme IDO2 is the preferred biochemical target of the antitumor indoleamine 2,3-dioxygenase inhibitory compound D-1-methyl-tryptophan. Cancer Res. 2007; 67:7082–7087. [PubMed: 17671174]
25. Opitz CA, Litzenburger UM, Sahm F, Ott M, Tritschler I, Trump S, et al. An endogenous tumour-promoting ligand of the human aryl hydrocarbon receptor. Nature. 2011; 478:197–203. [PubMed: 21976023]
26. Bunt SK, Yang L, Sinha P, Clements VK, Leips J, Ostrand-Rosenberg S. Reduced inflammation in the tumor microenvironment delays the accumulation of myeloid-derived suppressor cells and limits tumor progression. Cancer Res. 2007; 67:10019–10026. [PubMed: 17942936]
27. Kim MY, Oskarsson T, Acharyya S, Nguyen DX, Zhang XH, Norton L, et al. Tumor self-seeding by circulating cancer cells. Cell. 2009; 139:1315–1326. [PubMed: 20064377]
28. Luo J, Solimini NL, Elledge SJ. Principles of cancer therapy: oncogene and nononcogene addiction. Cell. 2009; 136:823–837. [PubMed: 19269363]
29. Prendergast GC. Immune escape as a fundamental trait of cancer: focus on IDO. Oncogene. 2008; 27:3889–3900. [PubMed: 18317452]
30. Munn DH, Zhou M, Attwood JT, Bondarev I, Conway SJ, Marshall B, et al. Prevention of allogeneic fetal rejection by tryptophan catabolism. Science. 1998; 281:1191–1193. [PubMed: 9712583]
31. Nonaka H, Saga Y, Fujiwara H, Akimoto H, Yamada A, Kagawa S, et al. Indoleamine 2,3-dioxygenase promotes peritoneal dissemination of ovarian cancer through inhibition of natural killercell function and angiogenesis promotion. Int J Oncol. 2011; 38:113–120. [PubMed: 21109932]
32. Li Y, Tredget EE, Ghaffari A, Lin X, Kilani RT, Ghahary A. Local expression of indoleamine 2,3-dioxygenase protects engraftment of xenogeneic skin substitute. J Invest Dermatol. 2006; 126:128–136. [PubMed: 16417228]

33. Uyttenhove C, Pilotte L, Theate I, Stroobant V, Colau D, Parmentier N, et al. Evidence for a tumoral immune resistance mechanism based on tryptophan degradation by indoleamine 2,3-dioxygenase. Nat Med. 2003; 9:1269–1274. [PubMed: 14502282]
34. Sharma MD, Hou DY, Liu Y, Koni PA, Metz R, Chandler P, et al. Indoleamine 2,3-dioxygenase controls conversion of Foxp3+ Tregs to TH17-like cells in tumor-draining lymph nodes. Blood. 2009; 113:6102–6111. [PubMed: 19366986]
35. Hu HM, Tian Q, Baer M, Spooner CJ, Williams SC, Johnson PF, et al. The C/EBP bZIP domain can mediate lipopolysaccharide induction of the proinflammatory cytokines interleukin-6 and monocyte chemoattractant protein-1. J Biol Chem. 2000; 275:16373–16381. [PubMed: 10748205]
36. DiNatale BC, Murray IA, Schroeder JC, Flaveny CA, Lahoti TS, Laurenzana EM, et al. Kynurenic acid is a potent endogenous aryl hydrocarbon receptor ligand that synergistically induces interleukin-6 in the presence of inflammatory signaling. Toxicol Sci. 2010; 115:89–97. [PubMed: 20106948]
37. Hodge DR, Hurt EM, Farrar WL. The role of IL-6 and STAT3 in inflammation and cancer. Eur J Cancer. 2005; 41:2502–2512. [PubMed: 16199153]
38. Kita H, Shiraishi Y, Watanabe K, Suda K, Ohtsuka K, Koshiishi Y, et al. Does Postoperative Serum Interleukin-6 Influence Early Recurrence after Curative Pulmonary Resection of Lung Cancer? Ann Thorac Cardiovasc Surg. 2011
39. Seow A, Ng DP, Choo S, Eng P, Poh WT, Ming T, et al. Joint effect of asthma/atopy and an IL-6 gene polymorphism on lung cancer risk among lifetime non-smoking Chinese women. Carcinogenesis. 2006; 27:1240–1244. [PubMed: 16344268]
40. DeMichele A, Martin AM, Mick R, Gor P, Wray L, Klein-Cabral M, et al. Interleukin-6-- 174G-->C polymorphism is associated with improved outcome in high-risk breast cancer. Cancer Res. 2003; 63:8051–8056. [PubMed: 14633738]
41. Ancrile B, Lim KH, Counter CM. Oncogenic Ras-induced secretion of IL6 is required for tumorigenesis. Genes and Development. 2007; 21:1714–1719. [PubMed: 17639077]
42. Angelo LS, Kurzrock R. Vascular endothelial growth factor and its relationship to inflammatory mediators. Clin Cancer Res. 2007; 13:2825–2830. [PubMed: 17504979]
43. Grivennikov SI, Karin M. Inflammatory cytokines in cancer: tumour necrosis factor and interleukin 6 take the stage. Ann Rheum Dis. 2011; 70(Suppl 1):i104–i108. [PubMed: 21339211]
44. Ostrand-Rosenberg S, Sinha P. Myeloid-derived suppressor cells: linking inflammation and cancer. J Immunol. 2009; 182:4499–4506. [PubMed: 19342621]
45. Bunt SK, Sinha P, Clements VK, Leips J, Ostrand-Rosenberg S. Inflammation induces myeloid-derived suppressor cells that facilitate tumor progression. J Immunol. 2006; 176:284–290. [PubMed: 16365420]
46. Sinha P, Clements VK, Fulton AM, Ostrand-Rosenberg S. Prostaglandin E2 promotes tumor progression by inducing myeloid-derived suppressor cells. Cancer Res. 2007; 67:4507–4513. [PubMed: 17483367]
47. Song X, Krelin Y, Dvorkin T, Bjorkdahl O, Segal S, Dinarello CA, et al. CD11b+/Gr-1+ immature myeloid cells mediate suppression of T cells in mice bearing tumors of IL-1beta-secreting cells. J Immunol. 2005; 175:8200–8208. [PubMed: 16339559]
48. Shirey KA, Jung JY, Maeder GS, Carlin JM. Upregulation of IFN-gamma receptor expression by proinflammatory cytokines influences IDO activation in epithelial cells. J Interferon Cytokine Res. 2006; 26:53–62. [PubMed: 16426148]
49. Heinrich PC, Behrmann I, Haan S, Hermanns HM, Muller-Newen G, Schaper F. Principles of interleukin (IL)-6-type cytokine signalling and its regulation. Biochem J. 2003; 374:1–20. [PubMed: 12773095]
50. Orabona C, Belladonna ML, Vacca C, Bianchi R, Fallarino F, Volpi C, et al. Cutting edge: silencing suppressor of cytokine signaling 3 expression in dendritic cells turns CD28-Ig from immune adjuvant to suppressant. J Immunol. 2005; 174:6582–6586. [PubMed: 15905495]
51. Orabona C, Pallotta MT, Volpi C, Fallarino F, Vacca C, Bianchi R, et al. SOCS3 drives proteasomal degradation of indoleamine 2,3-dioxygenase (IDO) and antagonizes IDOdependent tolerogenesis. Proc Natl Acad Sci USA. 2008; 105:20828–20833. [PubMed: 19088199]

52. Fasbender A, Lee JH, Walters RW, Moninger TO, Zabner J, Welsh MJ. Incorporation of adenovirus in calcium phosphate precipitates enhances gene transfer to airway epithelia in vitro and in vivo. J Clin Invest. 1998; 102:184–193. [PubMed: 9649572]

53. Sinha P, Clements VK, Ostrand-Rosenberg S. Reduction of myeloid-derived suppressor cells and induction of M1 macrophages facilitate the rejection of established metastatic disease. J Immunol. 2005; 174:636–645. [PubMed: 15634881]

STATEMENT OF SIGNIFICANCE

This study provides preclinical, genetic proof of concept that the immune regulatory enzyme IDO contributes to autochthonous carcinoma progression and to the creation of a metastatic niche. IDO deficiency *in vivo* negatively impacted both vascularization and IL6-dependent, MDSC-driven immune escape, establishing IDO as an overarching factor directing the establishment of a pro-tumorigenic environment.

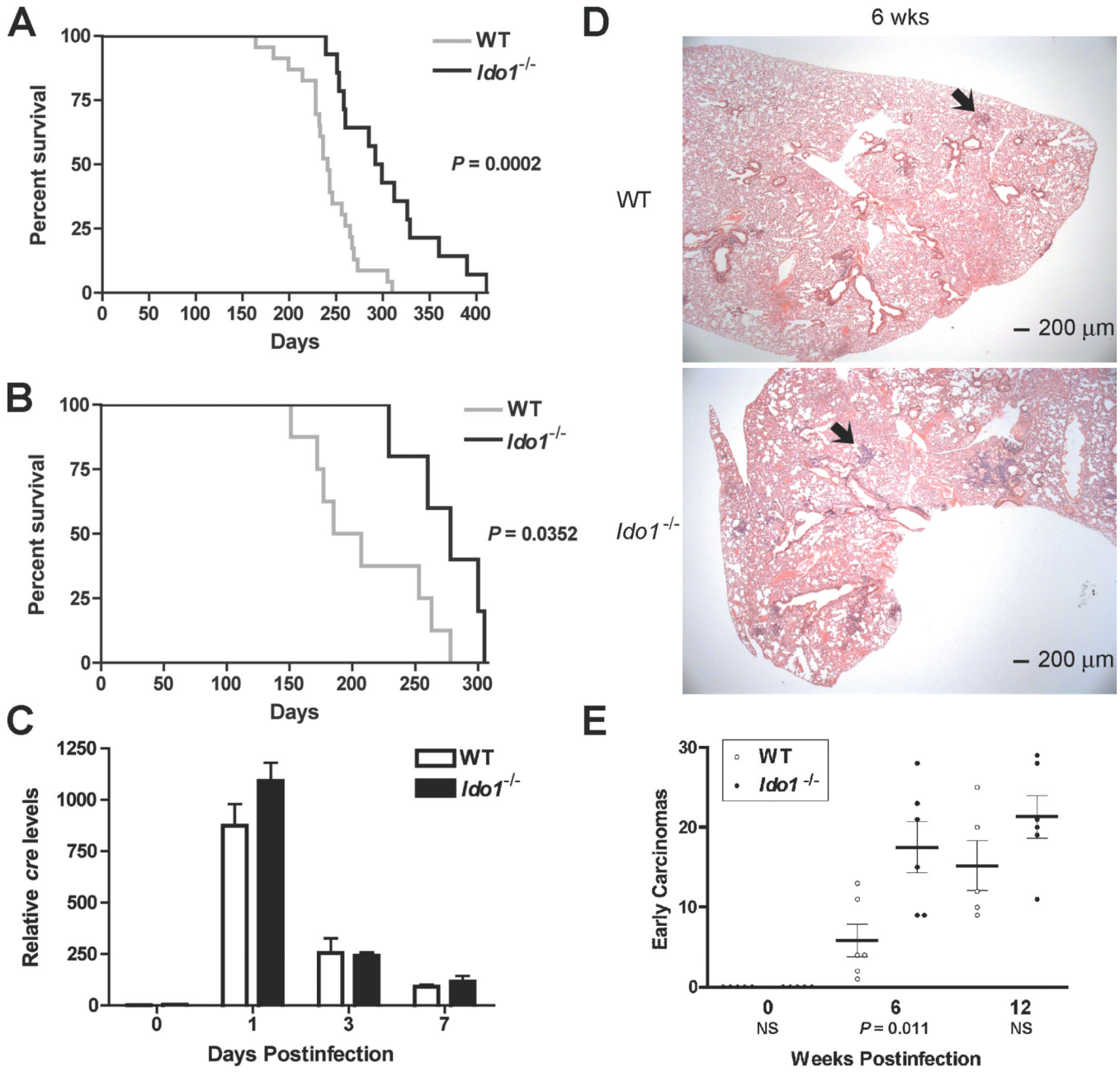

Figure 1.

IDO-deficiency extends the survival of mice with KRAS-induced lung adenocarcinomas despite an elevated number of early lesions. (**A**) Kaplan-Meier survival curves for cohorts of *Lox-Kras*^{G12D} ($N = 23$) and *Ido1*$^{-/-}$ *Lox-Kras*^{G12D} ($N = 14$) mice infected with 2.5×10^7 PFU Ad-*cre* virus. (**B**) Kaplan-Meier survival curves for cohorts of *Lox-Kras*^{G12D} ($N = 8$) and *Ido1*$^{-/-}$ *Lox-Kras*^{G12D} ($N = 5$) mice infected with 1.25×10^8 PFU Ad-*cre* virus. Significance for both data sets was assessed by 2-group log-rank test at $P < 0.05$. (**C**) Total lung DNA prepared from 3 mice per time point was analyzed for the presence of the viral *cre* gene by real time PCR at 0, 1, 3, 7 days postinfection. Relative *cre* levels determined from this analysis are plotted as means ± SEM. (**D**) Representative H&E stained sections depicting the observed difference in early lesions between the lungs of *Lox-Kras*^{G12D} and *I*

d o 1$^{-/-}$ *Lox-Kras*^{G12D} mice at 6 weeks postinfection. (**E**) Quantitative histopathological assessment of lesion frequency in H&E stained sections of lung biopsies from *Lox-Kras*^{G12D} and *Ido1*$^{-/-}$ *Lox-Kras*^{G12D} mice at 6wk and 12wk postinfection ($N \geq 5$). The number of lesions identifiable under low magnification within a defined region of each specimen are graphed on the scatter plot with the means ± SEM. Significance was determined by two-tailed Student's *t* test at $P < 0.05$) (NS; not significant).

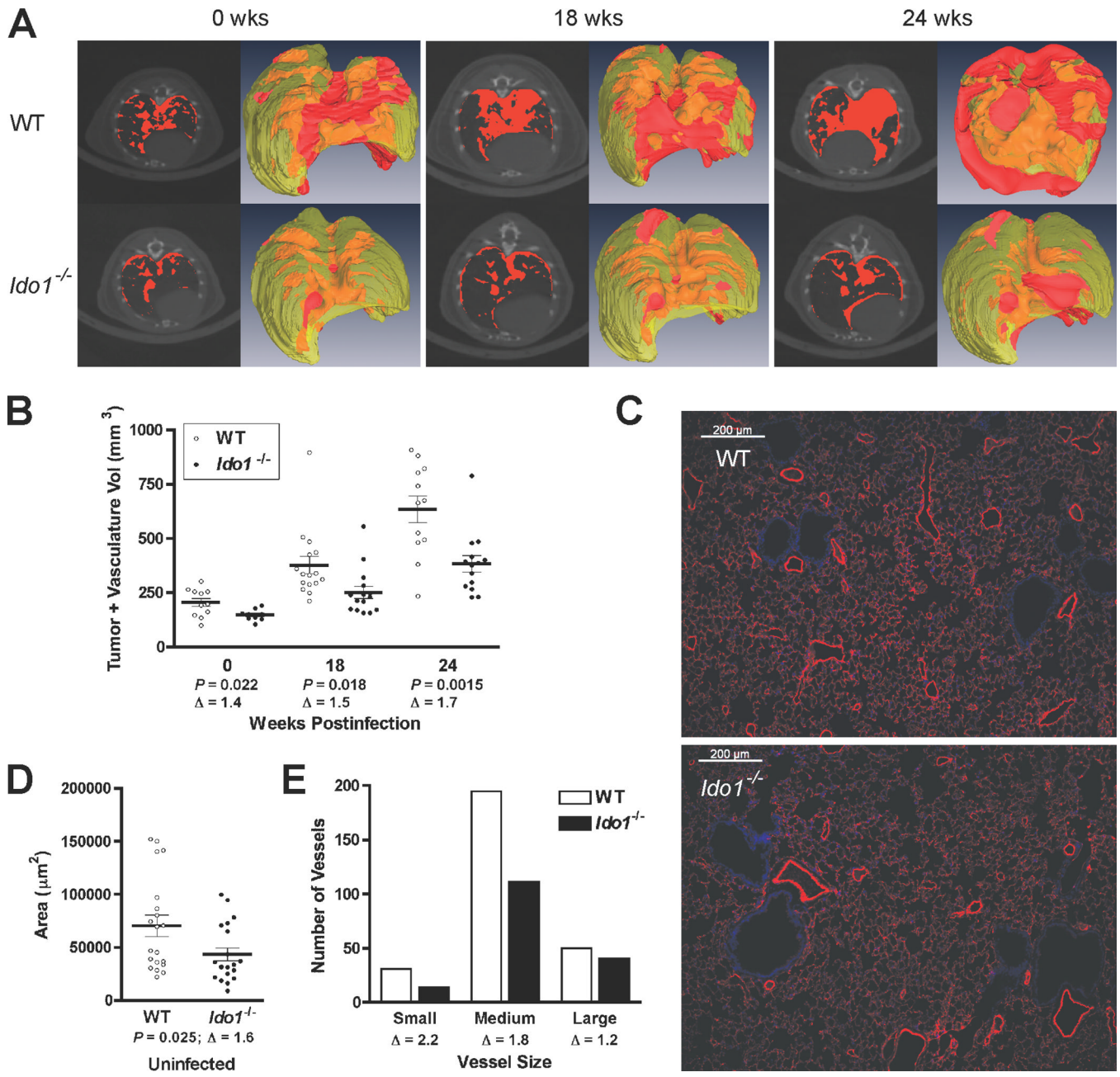

Figure 2.

IDO-deficiency impairs the outgrowth of overt lung adenocarcinomas and reduces normal pulmonary vascularization. (**A**) Representative axial micro-CT images and 3-D reconstructions of *Lox-Kras*^{G12D} and *Ido1*$^{-/-}$ *Lox-Kras*^{G12D} mouse lungs acquired at 0, 18 and 24 weeks post-infection. Tumor and vasculature, which have indistinguishable X-ray densities, are designated in red in the individual CT images (*left panels*) or red/orange for exterior/interior location in the 3-D reconstructions (*right panels*). (**B**) Volumetric image analysis of tumor and vasculature performed on the 3-D reconstructions of lung micro-CT images. The data are graphed as a scatter plot with the means ± SEM (Δ; fold difference). Significance was determined by two-tailed Student's *t* test at $P < 0.05$. (**C**) Immunofluorescent staining of blood vessels with antibody to caveolin 1 (red) and DAPI

staining of nuclei (blue) in representative lung tissue specimens from WT and *Ido1*$^{-/-}$ mice. (**D**) Quantitation of blood vessel areas. The vessel area totals measured within each field are graphed as a scatter plot with the means ± SEM (Δ; fold difference). Significance was determined by two-tailed Student's *t* test at $P < 0.05$. (**E**) Distribution of pulmonary vessels within specified size ranges. The total number of small (<500 μm^2), medium (500–5000 μm^2) and large (>5000 μm^2) vessels identified within the defined fields evaluated in D are plotted on a bar graph (Δ; fold difference). Also see Supplementary Fig. S1C for a graph of individual vessel measurements rank ordered across the entire size range.

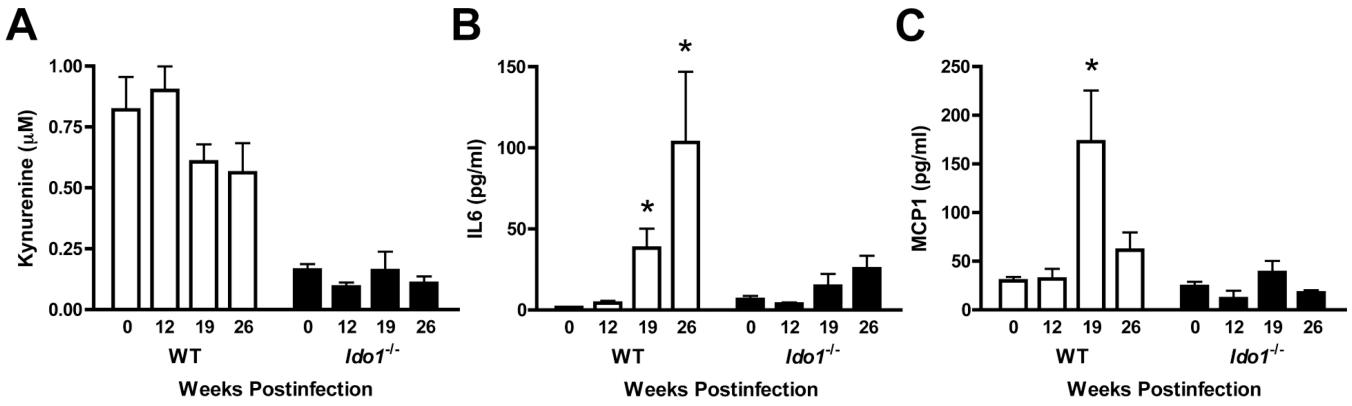

Figure 3.

IDO-deficiency is associated with attenuated induction of IL6 and MCP1. (**A**) Kynurenine levels in the lungs of *Lox-Kras*^{G12D} and *Ido1*$^{-/-}$ *Lox-Kras*^{G12D} mice at 0, 12, 19, and 26 weeks post-infection ($N \geq 3$) assessed by liquid chromatography-tandem mass spectroscopy analysis and plotted as the means ± SEM. (**B,C**) IL6 and MCP1 levels in the lungs of *Lox-Kras*^{G12D} and *Ido1*$^{-/-}$ *Lox-Kras*^{G12D} mice at 0, 12, 19, and 26 weeks postinfection ($N \geq 3$) assessed by multiplexed cytokine bead immunoassay-based analysis and plotted as the means ± SEM with significance relative to baseline determined by 1-way ANOVA with Dunn's test (*; $P < 0.05$).

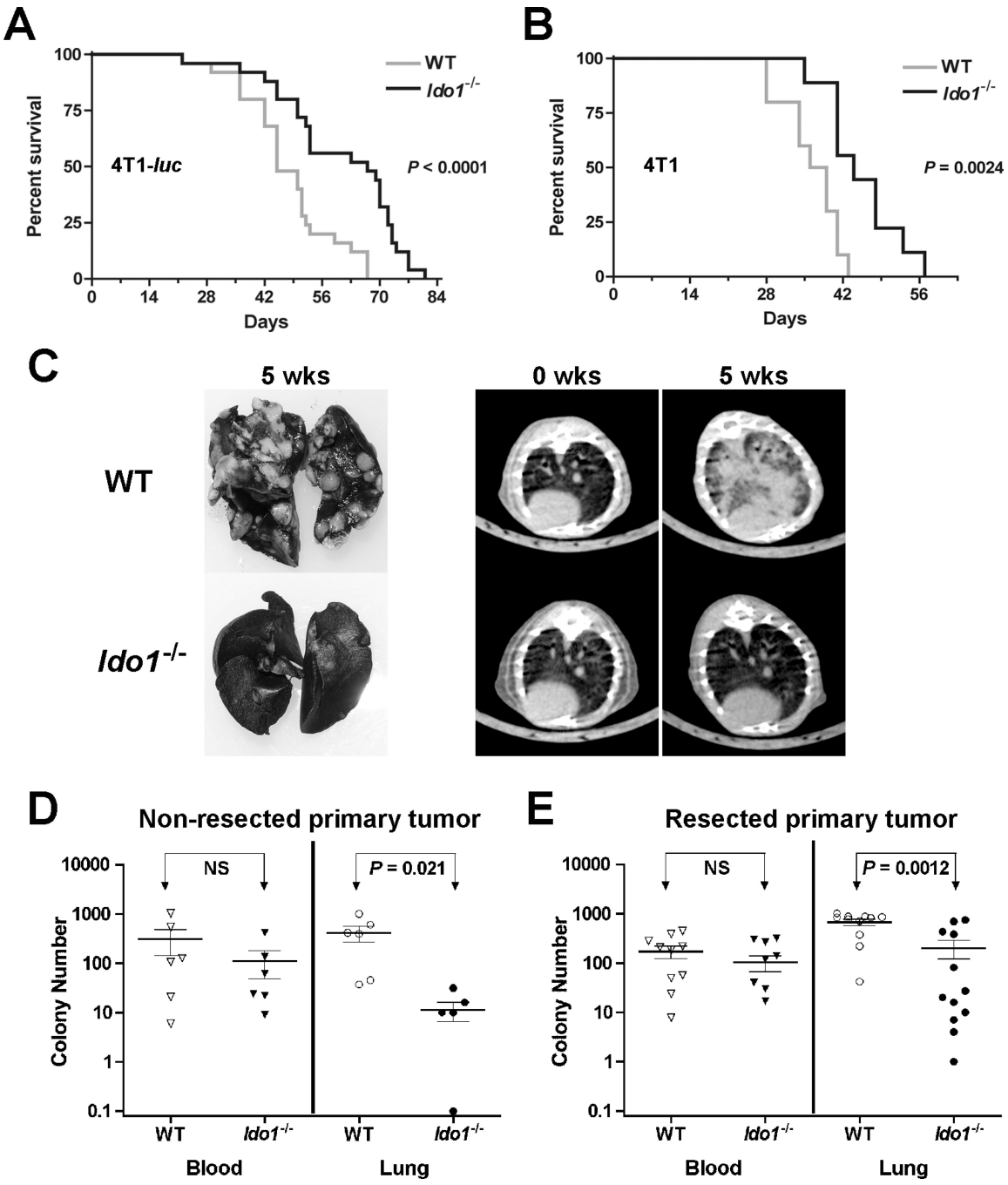

Figure 4.

IDO-deficiency delays the development of pulmonary metastases. Kaplan-Meier survival curves for cohorts of WT and *Ido1*$^{-/-}$ mice following orthotopic engraftment of 1×10^4 (**A**) 4T1-luc ($N = 25$) or (**B**) 4T1 ($N \geq 9$) tumor cells. Significance was assessed by 2-group log-rank test at $P < 0.05$. The survival benefit observed in *Ido1*$^{-/-}$ mice was independently replicated at UMBC. (**C**) Staining of lungs with India ink and axial images from micro-CT scans depicting the difference in pulmonary metastasis burden between WT and *Ido1*$^{-/-}$ mice at 5 weeks following orthotopic 4T1 tumor cell engraftment. At 5 weeks following (**D**) orthotopic engraftment of 4T1 cells ($N = 6$) or (**E**) orthotopic engraftment of 4T1 cells and

resection of the primary tumor at 18 days post-engraftment ($N \geq 11$), colony forming assays were performed to assess the relative tumor cell burden in the blood (neat) and lungs (1:1000). Individual data points are graphed on a log scale scatter plot with the means ± SEM and significance assessed by two-tailed Student's *t* test at $P < 0.05$ (NS; not significant).

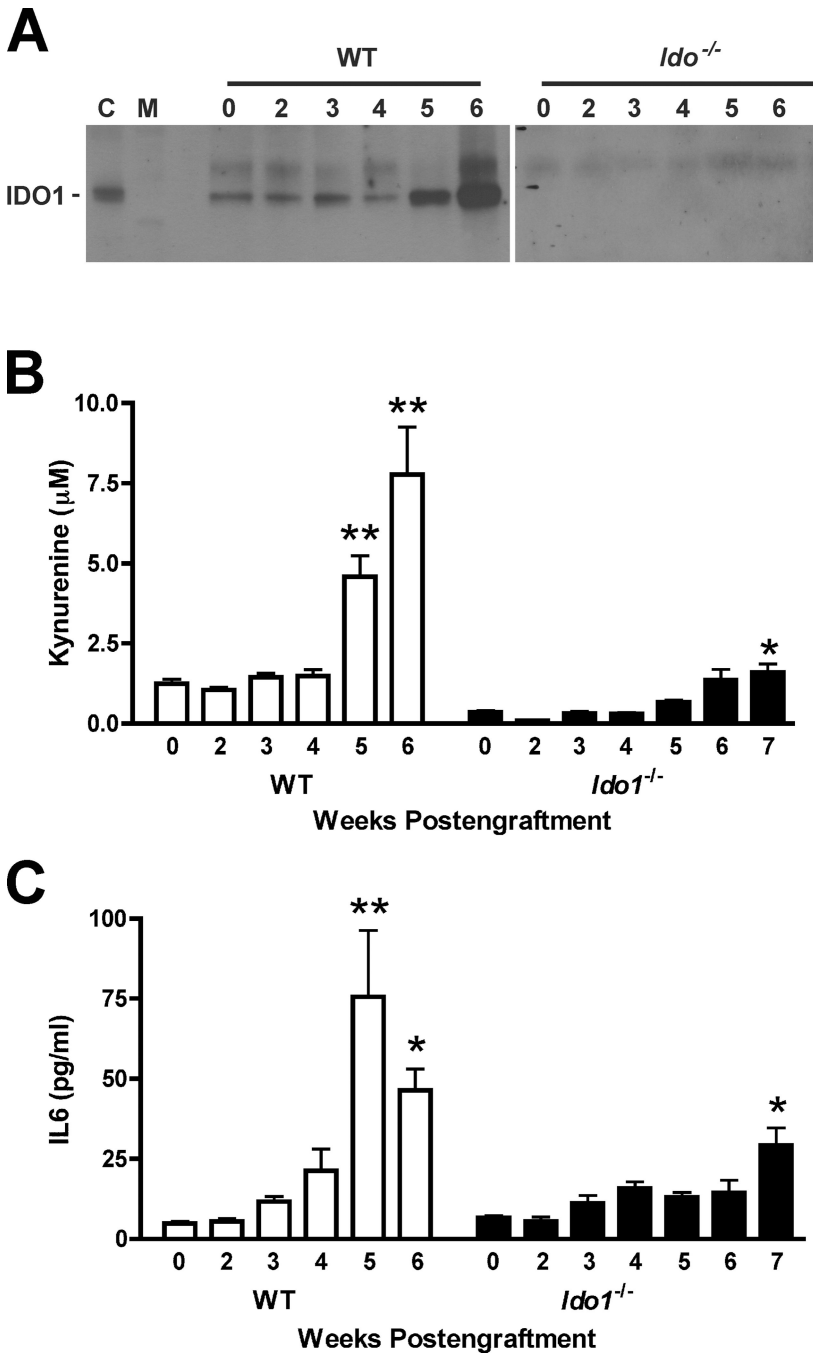

Figure 5.

IDO-deficiency is associated with attenuated induction of IL6 during 4T1 tumor metastasis. (**A**) Evaluation of IDO1 protein levels by IP-Western blot analysis of lung tissue lysates from WT and *Ido1*$^{-/-}$ mice following orthotopic engraftment of 4T1 tumor cells at the time points in weeks indicated above each lane, [C; epididymis lysate positive control lane, M; molecular weight marker lane]. (**B**) Evaluation of kynurenine levels by liquid chromatography-tandem mass spectroscopy-based analysis of homogenized lung samples from WT and *Ido1*$^{-/-}$ mice following orthotopic engraftment of 4T1 tumor cells at the time points in weeks indicted for each lane. Means ± SEM ($N \geq 6$) are graphed with significance

relative to baseline determined by 1-way ANOVA with Dunn's test (*; $P < 0.05$, **; $P < 0.01$). (**C**) IL6 level determinations from cytokine bead array immunoassay-based analysis of homogenized lung samples from WT and *Ido1*$^{-/-}$ mice following orthotopic engraftment of 4T1 tumor cells at the time points in weeks indicted for each lane. Means ± SEM ($N \geq 3$) are graphed with significance relative to baseline determined by 1-way ANOVA with Dunn's test (*; $P < 0.05$, **; $P < 0.01$).

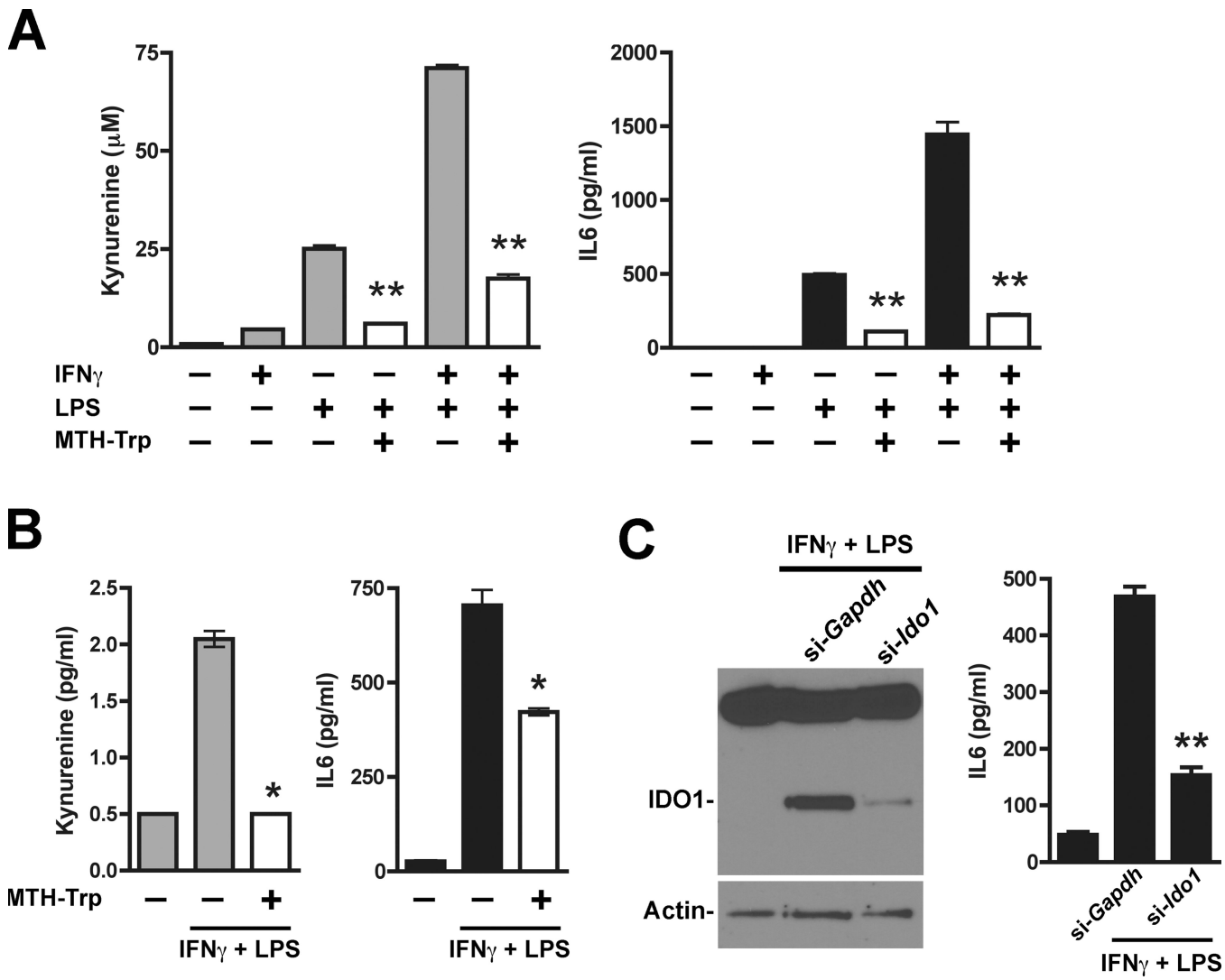

Figure 6.

IDO-dependent potentiation of IL6 production. (**A**) Supernatant from U937 cells stimulated for 24 hours with IFNγ (100 ng/ml) and/or LPS (100 ng/ml) was analyzed for kynurenine and IL6. Results from triplicate wells are plotted as the means ± SEM. Methyl thiohydantoin tryptophan (MTH-Trp, 100 μmol/l) was included during induction where indicated and significance relative to the corresponding induced level without MTH-Trp was determined by two-tailed Student's *t* test (**; $P \leq 0.0001$). (B) Supernatant from HL-60 cells stimulated for 24 hours with IFNγ (100 ng/ml) and LPS (100 ng/ml) was analyzed for kynurenine and IL6. Results from duplicate wells are plotted as the means ± SEM. Methyl thiohydantoin tryptophan (MTH-Trp, 100 μmol/l) was included during induction where indicated and significance relative to the corresponding induced level without MTH-Trp was determined by two-tailed Student's *t* test (*; $P < 0.05$). (C) HL-60 cells treated in triplicate with *Ido1*-targeting (si-*Ido1*) or non-targeting (si-*Gapdh*) siRNAs were stimulated for 24 hours with IFNγ (100 ng/ml) and LPS (100 ng/ml). Pooled cell lysates were analyzed by Western blot analysis for IDO1 and β-actin (*left panel*). IDO1 induction was suppressed by approximately 89.7% as assessed by densitometry analysis and normalization to actin. Individual cell supernatants were analyzed for IL6 (*right panel*). The IL6 data are plotted as the means ±

SEM with the significance of the difference between specific *Ido1*-targeting versus non-targeting results determined by two-tailed Student's *t* test (**; $P < 0.0001$).

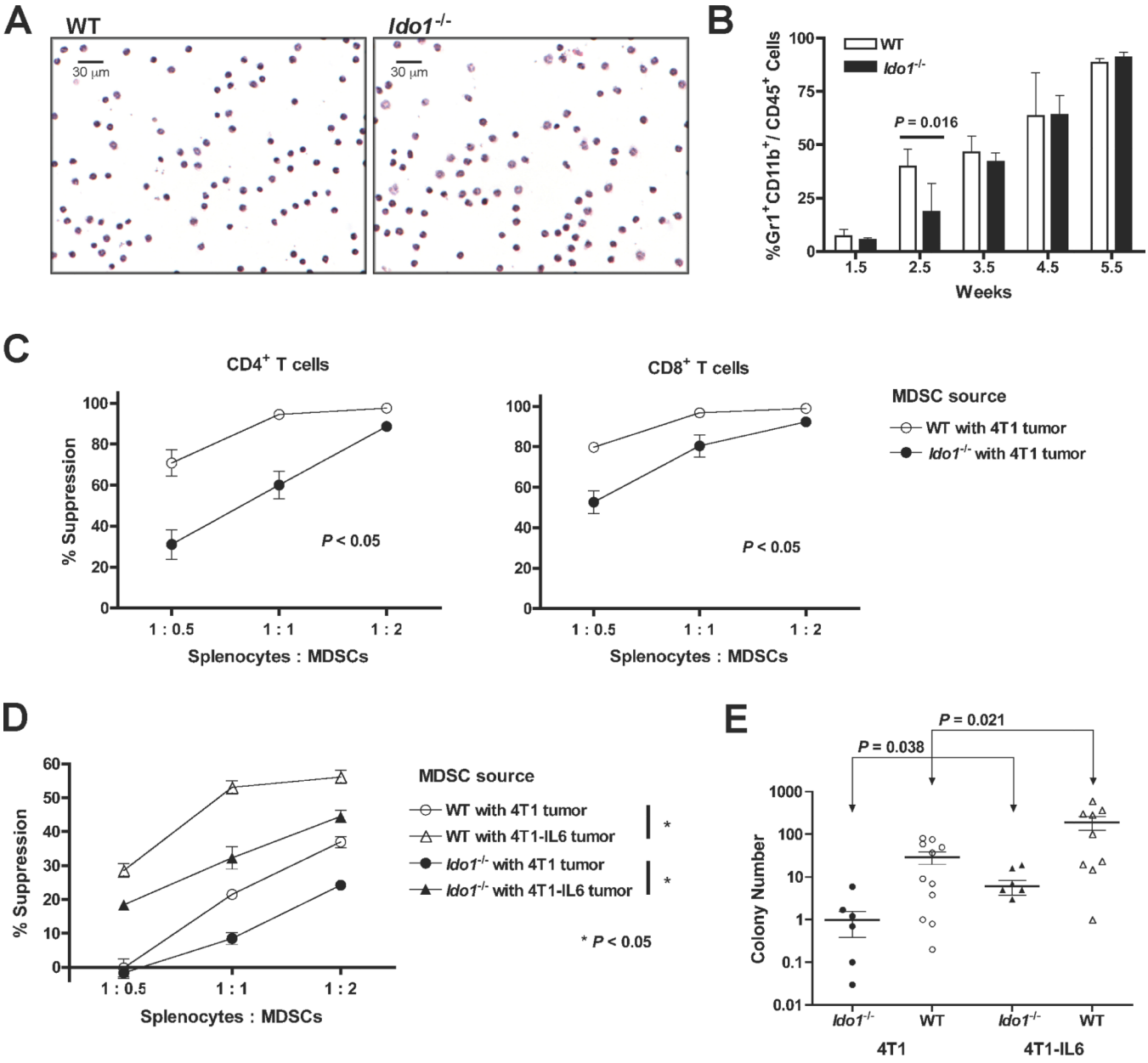

Figure 7.

Attenuated MDSC suppressive activity and metastasis development in IDO-deficient mice is rescued by IL6. (A) Comparative microscopic images of H&E-stained MDSCs harvested from the blood of WT and *Ido1*$^{-/-}$ mice with primary 4T1 tumors that were not significantly different in size (12.2 ± 1.36 and 11. 5± 0.4 mm in diameter, respectively). (**B**) Single cell suspensions of whole lung tissues were prepared at the indicated time points following 4T1 engraftment into WT and *Ido1*$^{-/-}$ mice and evaluated by flow cytometry for MDSC infiltration by gating on CD45^{+} cells and analyzing the Gr1^{+}CD11b^{+} cell population. Means ± SEM are graphed with significance assessed by two-tailed Student's *t* test at $P < 0.05$. (**C**) Splenocytes from CD4^{+} TS1 (*left*) or CD8^{+} Clone 4 (*right*) mice were co-cultured in triplicate with cognate peptide and increasing proportions of 4T1-induced, peripheral blood MDSCs from WT or *Ido1*$^{-/-}$ mice. T cell activation was quantified by uptake of ^{3}H-thymidine and graphed as percent suppression relative to activation in the absence of

MDSCs. Significance was assessed by Wilcoxon Rank test at $P < 0.05$. Outcomes are representative of a minimum of 3 independent experiments. (**D**) Splenocytes from $CD8^+$ Clone 4 transgenic mice were co-cultured with cognate peptide and increasing proportions of 4T1 or 4T1-IL6 tumor-induced MDSCs from WT or *Ido1*$^{-/-}$ mice for analysis as in B. Outcomes are representative of 6 independent experiments using TS1, Clone 4, or DO11.10 transgenic T cells. (**E**) Colony forming assays to assess the relative tumor cell burden in the lungs performed 6 weeks following intravenous injection of 4T1 or 4T1-IL6 cells into WT and *Ido1*$^{-/-}$ mice. Results are presented on log scale scatter plot with means ± SEM. Significance was assessed by two-tailed Student's *t* test at $P < 0.05$.